ADVANCED MATERIALS
www.advmat.de

Liquid Metal Composites with Enhanced Thermal Conductivity and Stability Using Molecular Thermal Linker

Han Wang, Wenkui Xing, Shen Chen, Chengyi Song, Michael D. Dickey,* and Tao Deng**

Gallium-based liquid metal (LM) composite with metallic fillers is an emerging class of thermal interface materials (TIMs), which are widely applied in electronics and power systems to improve their performance. In situ alloying between gallium and many metallic fillers like copper and silver, however, leads to a deteriorated composite stability. This paper presents an interfacial engineering approach using 3-chloropropyltriethoxysilane (CPTES) to serve as effective thermal linkers and diffusion barriers at the copper-gallium oxide interfaces in the LM matrix, achieving an enhancement in both thermal conductivity and stability of the composite. By mixing LM with copper particles modified by CPTES, a thermal conductivity (κ) as high as 65.9 W m^{-1} K^{-1} is achieved. In addition, κ can be tuned by altering the terminal groups of silane molecules, demonstrating the flexibility of this approach. The potential use of such composite as a TIM is also shown in the heat dissipation of a computer central processing unit. While most studies on LM-based composites enhance the material performance via direct mixing of various fillers, this work provides a different approach to fabricate high-performance LM-based composites and may further advance their applications in various areas including thermal management systems, flexible electronics, consumer electronics, and biomedical systems.

1. Introduction

With the ever-increasing integration level of electronic devices and the escalatingpower density, the thermal management of many electronic devices becomes more and more crucial to ensure their reliable operations.[1,2] In particular, thermal interface materials (TIMs) act as an essential part of thermal management by enhancing the thermal coupling between interfaces of electronic devices to achieve efficient heat dissipation.[3] Traditional TIMs are polymer-based composite materials containing thermal conductive fillers. The polymer matrix endows TIMs flexibility to fill the air gaps at the interface. Their thermal performance, however, is generally limited by the poor thermal transport in polymers.[4]

Gallium-based liquid metals are promising candidates for high-performance TIMs.[5] Their metallic nature ensures an intrinsic high κ and good thermal transport performance. The fluidity of liquid metals enables them to fill the air gaps between the electronic chips and heat sinks. Such fluidity, however, may lead to leakage problems during operation.[6] The relatively high surface tension of liquid metal also makes it hard to be uniformly applied on the surface of electronic devices.[7] Adding solid fillers into the liquid metal matrix via mechanical mixing is an effective way to further increase the thermal conductivity of liquid metal composites while addressing the problem of leakage. During the mixing process in air, gallium-based liquid metal can be easily oxidized to generate a thin (approximately several nanometers) layer of amorphous gallium oxide (Ga_2O_3), which helps encapsulate solid fillers into the liquid metal matrix.[8,9] The formation of Ga_2O_3 also decreases the liquid metal surface tension, leading to better adhesion properties on various substrates. Such enhanced adhesion is especially useful to reduce the contact thermal resistance in the TIM application.[10] By changing the amount of solid filler, the mixture can be turned from liquid to paste-like, decreasing the possibility of leakage of liquid metal. The approach of adding solid particles into liquid metal has been used in many works for thermal management applications.[11–19] Wang et al. incorporated the diamond particles into liquid metal by direct mixing and achieved a thermal conductivity of > 100 W m^{-1} K^{-1} in both parallel and perpendicular directions. The huge average diameter of 250 um in particle size, however, impedes its application as effective TIM. Reduced graphene oxide was also used as a filler to mix with liquid metal in their work. The 2D structure of the filler ensured a smooth surface and good heat spread property (126 ± 3.1 W m^{-1} K^{-1} in the paralleled direction). However, it also led to the heat anisotropy of the composite, with a thermal conductivity of only 10.5 ± 2.3 W m^{-1} K^{-1} in the perpendicular direction.[12] Liu and his coworkers used the iron particles coated with the silver

H. Wang, W. Xing, S. Chen, C. Song, T. Deng
Center of Hydrogen Science, School of Materials Science and Engineering
Shanghai Jiao Tong University
800 Dong Chuan Road, Shanghai 200240, P. R. China
E-mail: chengyi2013@sjtu.edu.cn; dengtao@sjtu.edu.cn
M. D. Dickey
Department of Chemical and Biomolecular Engineering
North Carolina State University
911 Partners Way, Raleigh, NC 27695, USA
E-mail: mddickey@ncsu.edu
The ORCID identification number(s) for the author(s) of this article can be found under https://doi.org/10.1002/adma.202103104.

DOI: 10.1002/adma.202103104

shell to mix into liquid metal and successfully extended the stability of liquid metal composite with the thermal conductivity of 48.95 ± 0.79 W m^{-1} K^{-1}. The coating process, however, is relatively complex.[16] The mixing of highly thermal conductive metallic fillers, such as silver and copper, with the liquid metal matrix, also helps increase the thermal conductivity of liquid metal composites. For instance, copper particles mixed with eutectic gallium indium (EGaIn; 75% Ga; 25% In) in NaOH solution achieved a thermal conductivity of 50 W m^{-1} K^{-1}.[13] Copper nanoparticles incorporated into GaInSn (66% Ga; 22%In; 16%Sn) via an oxide-free ultrasonic-assisted internalization process in HCl solution reached a high κ of 64.8 W m^{-1} K^{-1}.[14] In these efforts involving mixing Ga-based liquid metal with fillers of high thermal conductivity, gallium, however, can react with many metals such as copper,[20,21] silver,[22] aluminum,[23] and iron,[16] to form intermetallic compounds (IMCs) due to its reactive nature. For example, in the eutectic gallium indium-copper (EGaIn-Cu) composite system, the reaction between copper and gallium produces $CuGa_2$ IMCs. The formation of such IMCs consumes gallium in the EGaIn matrix and results in a compositional shift and melting point increase since $CuGa_2$ IMC has a high melting point.[24] The above reaction leads to a gradual solidification of EGaIn-Cu composites. If the EGaIn surface oxide is chemically removed by NaOH (aq), copper and gallium will come into direct contact and $CuGa_2$ IMCs start to form within several minutes after mixing.[25] Due to the rapid alloying process, the as-synthesized EGaIn-Cu composites solidify within days and are unable to be used as an effective TIM.

Here we present an interfacial engineering approach to enhance both the thermal conductivity and stability of EGaIn-copper particle (EGaIn-CuP) composites, in which 3-chloropropyltriethoxysilane (CPTES) was used to chemically modify the surface of CuPs. CPTES molecules not only serve as effective thermal linkers at CuP/Ga_2O_3 interfaces to enhance the bulk thermal conductivity of the composite, but also promote the stability of composites by suppressing the formation of $CuGa_2$ IMCs. The thermal conductivity of EGaIn-CuP composites modified with the chlorine terminated silane (EGaIn-CuP@Cl) reaches as high as 65.9 W m^{-1} K^{-1}, which is among the highest value reported for gallium-based liquid metal composites with metallic fillers. We attribute the achievement of such high thermal conductivity to the enhancement of interfacial thermal conductance (κ_{int}) at CuP/Ga_2O_3 interfaces due to the electrostatic interaction of chlorine group in CPTES with gallium in the oxide layer. The CPTES modification decreases κ_{int} and acts as effective thermal linkers at CuP/Ga_2O_3 interfaces. Moreover, the silane molecules anchored on the surface of CuP also serve as a diffusion barrier between CuP and Ga_2O_3 layer. This diffusion barrier significantly suppresses the formation of $CuGa_2$ IMCs and effectively enhances the stability of EGaIn-CuP composites. The thermal conductivities of EGaIn-CuP composites using amino and thiol terminated silanes as modification agents have been studied as well to show that the bulk thermal conductivity can be tuned by altering the strength of chemical interactions at CuP/Ga_2O_3 interfaces. A CPU heat dissipation test was carried out to demonstrate the thermal performance of EGaIn-CuP@Cl composites as a TIM. While most of the studies on liquid metal-based composites enhance material performance through direct mixing of various fillers into liquid metals with no interfacial modification,[11–14] this study provides an alternative approach using interfacial engineering to serve as interfacial thermal linkers and diffusion barriers. This work not only offers a facile and versatile method for fabricating highly thermal conductive liquid metal composites with enhanced stability, but also provides a different approach for the fabrication of high-performance liquid metal composites, which may further advance their applications in various fields including thermal management systems,[26] flexible electronics,[27,28] consumer electronics,[14] and biomedical systems.[29]

2. Results and Discussion

The synthetic procedure of EGaIn-CuP@Cl is schematically summarized in **Figure 1**. Spherical CuP powder was pre-weighed and poured into a glass bottle with toluene, and a specific amount of CPTES was then added into the solution. The mixing process was carried out using an electrical shear blender. During the overnight incubation process, moisture in the ambient atmosphere,[30] the water absorbed on the inner container surface,[26] and the existing trace amount of water in toluene[31] reacted with the ethoxy groups in CPTES via hydrolysis reaction to form 3-chloropropylsilanetriol (CPST) and ethanol. The hydroxyl groups in CPST would further react with hydroxyl groups on the partially oxidized CuP surface via dehydration reaction.[32,33] Therefore, the silanes will be strongly attached to CuPs via covalent Si—O—Cu— bonds. After subsequent washing and drying, CuPs modified with CPTES (CuP@Cl) were synthesized and kept in storage for future use. The as-prepared CuP@Cl powder was then simply mixed with EGaIn in ambient conditions. The presence of Ga_2O_3 on EGaIn surface increases the adhesion of EGaIn to the CuPs. During the mixing process, the freshly generated Ga_2O_3 at the surface broke into pieces under shear force, making the unoxidized inner EGaIn surface exposed to the air and forming new oxide layers. Such oxide layers adhered to the CuPs and helped wrap CuPs into the EGaIn matrix.[11] Therefore, with the continuous exposure of fresh EGaIn surface and formation of new oxide layer under shear force, the filler particles could be incorporated into the EGaIn matrix via an oxide-assisted process, and a well-dispersed EGaIn-CuP composite was rapidly obtained. To demonstrate the oxide-assisted effect in this work, a parallel control experiment was conducted in the nitrogen atmosphere. Different from the mixture obtained in the oxygen-rich ambient atmosphere, due to the absence of oxygen and no formation of new surface oxide, the CuP@Cl particles and EGaIn could not form a homogeneous mixture (Figure S1, Supporting Information). The dissolution experiment of EGaIn-CuP@Cl composites in 1 M sodium hydride (NaOH) at room temperature also confirmed the oxide-assisted process (Figure S2, Supporting Information). Ga_2O_3 was readily dissolved in NaOH, while gallium and indium barely reacted with dilute NaOH at room temperature. After dropping the as-prepared liquid metal composite into the dilute NaOH solution, brown CuPs appeared due to the dissolution of gallium oxide wrapped on their surface and the phase separation occurred between the liquid metal and CuPs.

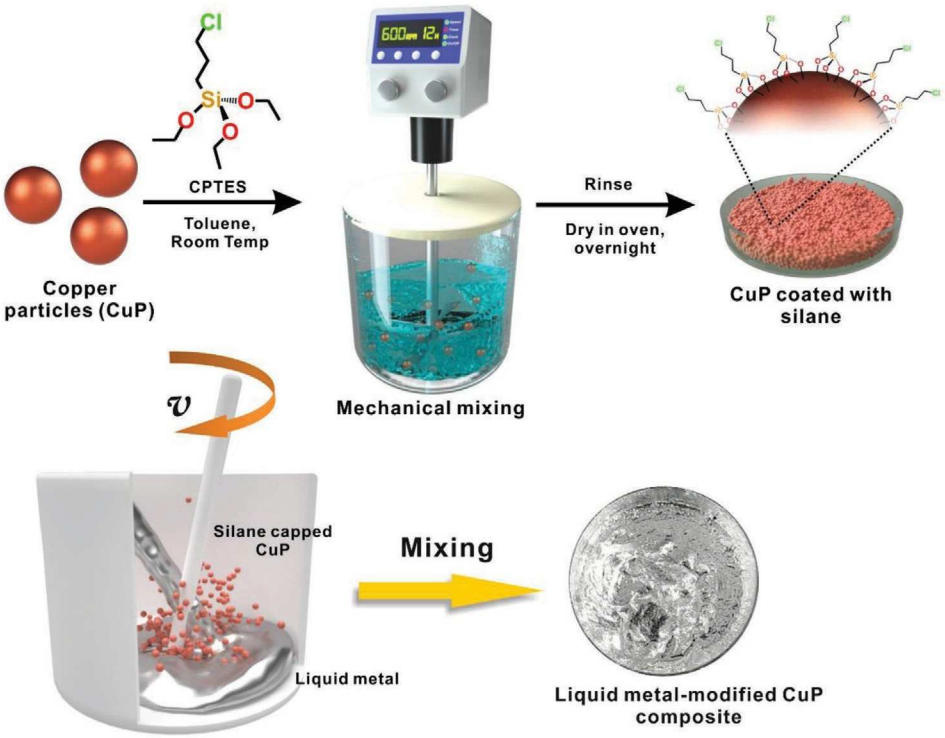

Figure 1. Schematic illustration for the generation of CPTES modified Cu particles and EGaIn-CuP@Cl composites.

As shown in **Figure 2a**, the optical image of CuPs after chemical modification shows no distinct difference in comparison with the unmodified CuPs. To characterize the CPTES modification on the surface of CuP, Fourier-transform infrared spectroscopy (FT-IR) was employed to identify the characteristic absorption peak of organic ligands attached to the CuP surface (Figure 2b). Two strong bands at 3445.6 cm^{-1} and 1634.7 cm^{-1} correspond to stretching and bending vibrational modes of water molecules, respectively.[34] The existence of water is not surprising since it may have been adsorbed on CuP@Cl particles from the ambient air during the synthesis or storage of the powder. The absorption peak at 2918 cm^{-1} corresponds to the C–H stretching vibration of the tetrahedron carbons in CPTES, indicating the existence of organic compounds on the surface of CuPs.[34] The broadband at 1076.1 cm^{-1} is attributed to the stretching vibration of the Si—O—Si bond[35] formed during the dehydration reaction of hydroxyl groups between neighboring CPTES.

To investigate the grafting situation of the silane organic layer, energy dispersive spectroscopy (EDS) mappings of the modified copper particles were conducted to gain insight into the coating uniformity of the silane molecules (Figure S3, Supporting Information). A relatively uniform distribution of the signal of characteristic elements (Cl for CuPs modified with Cl terminated silane), indicating the good uniformity of the silane coating.

X-ray photoelectron spectroscopy (XPS) was utilized to study the surface chemical state of the CuP@Cl. The high-resolution region scan of Cl 2p on CuP@Cl is shown in Figure 2c. Deconvoluted Cl 2p spectrum of CuP@Cl yields two doublets of Gaussian peaks. The doublet at 200.1 and 201.7 eV (Cl $2p_{3/2}$ and Cl $2p_{1/2}$) represents organic chlorine,[36] corresponding to the C—Cl bond structure in CPTES, whereas another doublet at 198.6 and 200.2 eV (Cl $2p_{3/2}$ and Cl $2p_{1/2}$) is related to metal chloride, which may be due to the possible interaction between Cl and Cu.[37] XPS was also employed to measure the thickness of the coated silane layer. The experiment was conducted by comparing the XPS spectra of unmodified CuP with CuP@Cl samples, and the thickness was approximated by evaluating the intensity attenuation of the Cu 2p core-level XPS signal.[38] Based on the XPS data and analysis (Figure S4, Supporting Information), we calculated that the thickness of organic silane layer to be 0.733 nm. Since the thickness of one such self-assembled monolayer is around 0.7 nm,[39] we believe that the structure of silane organic layer should be composed of a single layer of CPTES.

After mixing the as-prepared CuP@Cl with EGaIn, the mixture is converted from a liquid-like state with low viscosity to a paste-like state with high viscosity, as shown in the optical images of Figure 2a. This morphology transformation is mainly due to the continuous oxide formation during the mixing process.[40] Scanning electron microscopy (SEM) was employed to examine the micro-scale surface texture of liquid metal composite. Figure 2d shows the surface morphology of EGaIn-CuP@Cl composites with different volume fractions (vol%) of CuPs. With the increase of CuP volume fraction, the density of CuPs in the liquid metal matrix increases, and so does the surface roughness. The SEM image in Figure 2e reveals the rather smooth surface of EGaIn-CuP@Cl composites with 51% CuP volume fraction. The EDS images show that the spherical CuPs are uniformly dispersed in the EGaIn matrix. Additional EDS mapping images of Cl and O elements

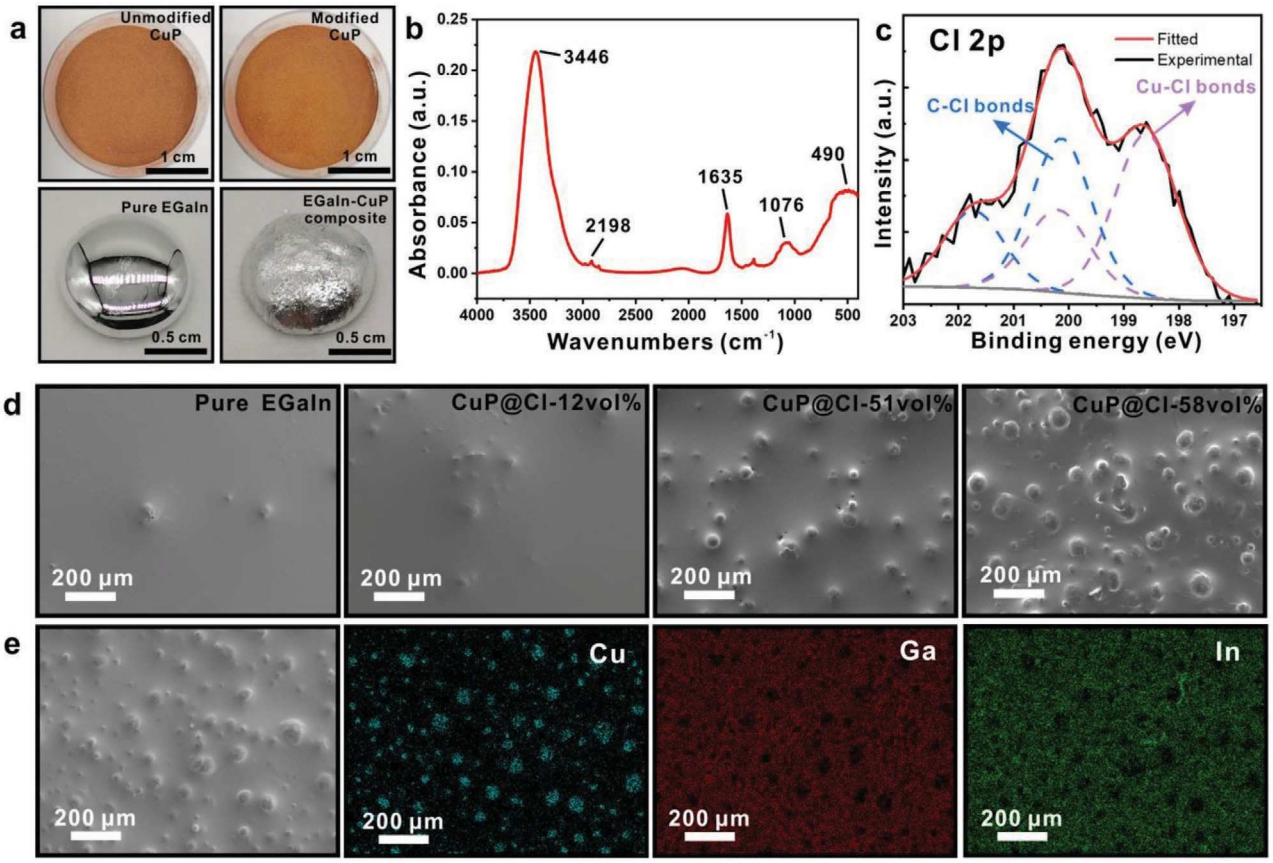

Figure 2. a) Optical images of modified and unmodified CuPs, pure EGaIn, and EGaIn-CuP-51 vol% composite. b) FT-IR spectra of chlorine-modified CuPs. c) High-resolution XPS Cl 2p spectra of CPTES modified CuPs. d) SEM images of pure EGaIn and EGaIn-CuP@Cl composites with different volume fractions of CuPs. e) EDS mapping and the corresponding SEM image of EGaIn-CuP@Cl-51 vol% composites showing the distribution of Cu, Ga, and In, elements, respectively.

are shown in Figure S5, Supporting Information. Micro-computed tomography (Micro-CT) analysis was also employed to interpret the inner structure of the EGaIn-CuP@Cl-51 vol% composites (Figure S6, Supporting Information). The region with shallow color is indicative of the liquid metal matrix. The darker spheres represent the spherical CuPs. The black holes in the Micro-CT images represent air pockets in the LM composites, which may be introduced during the mixing process in air. The total area fraction of air pockets to the whole liquid metal composite was measured to be 2.2%. It has been taken as the porosity to build our heat transfer model in the following section.

The thermal performance of EGaIn-CuP composites was also investigated. **Figure 3a** outlines the thermal conductivity of EGaIn-CuP@Cl composites and unmodified EGaIn-CuP composites as a function of CuP volume fraction. For EGaIn-CuP composites, with the gradual increase of CuP volume fraction, the thermal conductivity increases first, but once the CuP volume fraction exceeds a certain threshold, the thermal conductivity starts to decrease. The thermal conductivity peaks at a filler volume fraction of 51%, with an average value of 57.0 ± 1.81 W m^{-1} K^{-1}. Such behavior can be attributed to the competition effect between copper filler with high thermal conductivity (401 W m^{-1} K^{-1}) and Ga_2O_3 flakes with low thermal conductivity (0.1–0.3 W m^{-1} K^{-1}).[11] When the copper volume fraction is low, the impact of an increasing amount of oxide toward the bulk thermal conductivity is negligible compared to the thermal conductivity enhancement from CuPs, increasing composite thermal conductivity in Figure 3a. However, when the CuP volume fraction exceeds a certain threshold, the increased generation of Ga_2O_3 reduces the overall thermal conductivity of the liquid metal matrix by consuming EGaIn. Such a decrease in matrix thermal conductivity overweighs the positive effect of CuPs, which leads to the decrease in bulk thermal conductivity in the latter stage of the curve.

The thermal conductivity of EGaIn-CuP@Cl composites as a function of CuP volume fraction shows a similar trend as EGaIn-CuP composites. The thermal conductivity of EGaIn-CuP@Cl, however, exhibits an overall enhancement in comparison with EGaIn-CuP composites at all volume fractions and even reaches an average value of 64.8 ± 1.05 W m^{-1} K^{-1} at 51 vol%. We hypothesize that this enhanced thermal performance of EGaIn-CuP@Cl composite is owing to the effect of interfacial thermal conductance (κ_{int}) enhancement at CuP/Ga_2O_3 (metal-dielectric) interface after the introduction of CPTES as capping reagent. It is known that κ_{int} is mainly affected by the interfacial bonding strength and phonon vibrational spectra mismatch between two interface materials.[42–44]

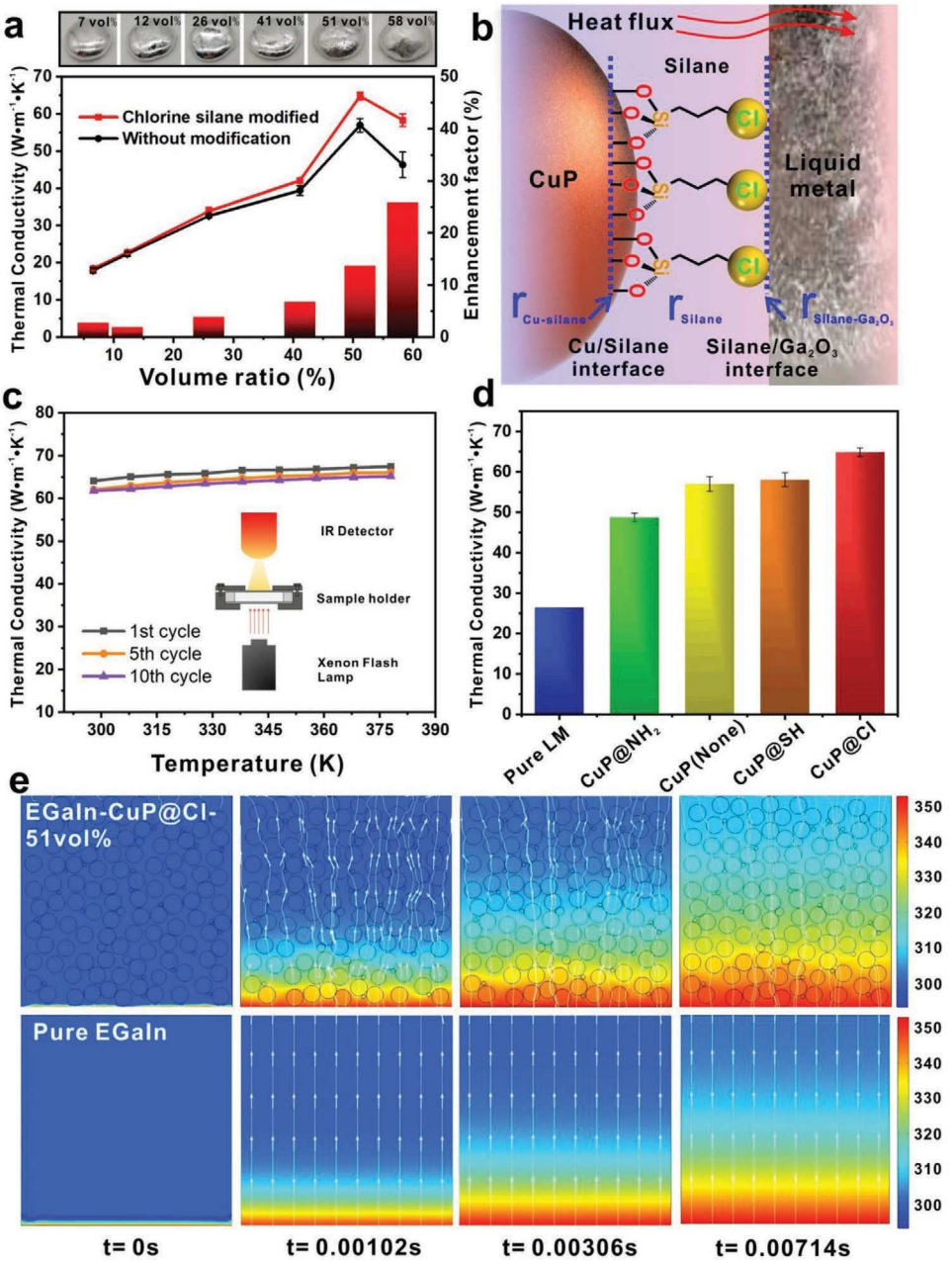

Figure 3. Thermal properties of EGaIn-CuP composites. a) Thermal conductivity of EGaIn-CuP@Cl composites and EGaIn-CuP composites as a function of CuP volume fraction, respectively. Thermal conductivity enhancement factors of EGaIn-CuP@Cl composites toward EGaIn-CuP composites are shown in the histogram form. Composite morphologies with different Cu volume fractions are shown on the top, exhibiting a trend from liquid rheology to viscous paste-like rheology. b) Schematic illustration of heat conduction at CuP/Ga_2O_3 interface in EGaIn-CuP@Cl composites. c) Cyclic thermal stability of EGaIn-CuP@Cl-51 vol% composites from 298 to 378 K. The inserted image is a schematic illustration of the laser flash analysis (LFA) measurement process. d) Thermal conductivity of pure liquid metal,[41] EGaIn-CuP-51 vol% composite, and EGaIn-CuP-51 vol% composites using CuPs modified with amino, thiol, and chlorine terminated silane. e) Finite element analysis on the thermal conduction showing the heat flux transport within pure EGaIn and EGaIn-CuP@Cl-51 vol% composites, respectively.

For amorphous materials, the investigation of phonon spectra is difficult since the definition of phonons becomes questionable when there is a lack of periodicity and a wave vector.[45] The Ga_2O_3 generated by direct oxidation in the air has an amorphous structure,[46,47] which implies disordered organization of atoms within such layer. Therefore, here we mainly focus on the impact of interfacial bonding effect on κ_{int}. The interfacial thermal resistance (r_{int}) between Cu and Ga_2O_3 inside the EGaIn-CuP@Cl system consists of three components (Figure 3b):

$$r_{int} = r_{Cu\text{-}silane} + r_{silane} + r_{silane\text{–}Ga_2O_3} \quad (1)$$

Of these sources of interfacial resistance, the value of $r_{Cu\text{-}Silane}$ should be relatively smaller because of the strong

covalent Si—O—Cu bonding between copper and silane.[42,48] Besides, the short and well-aligned silane molecules are usually of high thermal conductance and contribute negligibly to the whole thermal interface resistance.[49–51] Consequently, we expect $r_{\text{Silane-Ga2O3}}$ to play a key role in the interfacial thermal resistance between Cu and Ga_2O_3 inside the EGaIn-CuP@Cl system. Chlorine is in the upper-right of the element periodic table and has a high electronegativity. Hence, the chlorine terminus in the silane is a strong Lewis acid and has a strong electron-withdrawing effect, which enables it to have strong electrostatic interaction with gallium in Ga_2O_3.[52] This rather strong electrostatic interaction may play a major role in constructing effective molecular thermal linkers to decrease r_{int} between Cu and Ga_2O_3, which results in the bulk thermal conductivity enhancement of EGaIn-CuP@Cl composites.[53] The thermal conductivity enhancement factor of EGaIn-CuP@Cl composites toward EGaIn-CuP composites shown in Figure 3a also confirms our supposition: The enhancement factor gradually increases from 1.13% to a final value of 25.89% with the increasing CuP volume fraction. Such an increase can be appropriately explained from the perspective of r_{int} difference at CuP/Ga_2O_3 interfaces. As the number of CuP/Ga_2O_3 interfaces levels up at high CuP volume fractions, the positive effect of reduced r_{int} at CuP/Ga_2O_3 interfaces toward bulk thermal conductivity can be enlarged, corresponding to an enhanced thermal conductivity. This thermal conductivity enhancement effect can also be observed by using CuP with a smaller average diameter of 21.5 µm. The thermal conductivity has achieved a 19.24% enhancement factor by comparing EGaIn-CuP@Cl composites (34.3 W m^{-1} K^{-1}) with EGaIn-CuP composites (28.9 W m^{-1} K^{-1}) at 51% CuP volume fraction.

The cyclic thermal conductivity measurement of EGaIn-CuP@Cl-51 vol% composite in the temperature range from 298 K to 378 K was performed (Figure 3c) to examine its thermal stability. After the initial decrease of ≈3%, the thermal conductivity stays relatively stable. Additionally, XRD spectra also confirm that there were no distinguished changes to the $CuGa_2$ peaks after thermal cycling (Figure S7, Supporting Information). The inserted image shows a schematic illustration of LFA measurement device consisting of a xenon laser flash lamp, sample mold, and IR detector. The detailed measurement process of thermal diffusivity using LFA is discussed in the supporting information.

The long-term thermal conductivity of EGaIn-CuP@Cl-51vol% composites was measured as well to illustrate the long-term thermal conductivity variation (Figure S8, Supporting Information). Initially, we observed a continuous increase in thermal conductivity of as-prepared LM composites from 1 to 6 days. It is attributed to the phase separation and the formation of $CuGa_2$ IMCs with relatively high thermal conductivity (103.6 W m^{-1} K^{-1}).[54] Eventually, the thermal conductivity reached a relatively stable value of ≈72.0 W m^{-1} K^{-1}. This trend of long-term thermal conductivity variation is also consistent with the report in the published work.[13]

To further validate our hypothesis that the difference in κ_{int} plays the key role for thermal conductivity enhancement in composites with modified and unmodified CuPs, CuPs capped with thiol (SH) and amino (NH_2) terminated silane were also synthesized. The EDS and XPS analysis of these CuPs are provided in the supporting information (Figures S3 and S9, Supporting Information). The liquid metal composites using thiol and amino terminated silane molecules as capping agents are abbreviated as EGaIn-CuP@SH and EGaIn-CuP@NH_2, respectively. We expect such composites to exhibit different thermal conductivity since the interaction strength between different terminal groups of silane molecules and Ga_2O_3 are different. The thermal conductivities of these composites at the same volume fraction of 51% are listed in Figure 3d. This thermal conductivity variation might be attributed to different bonding strengths, that is, different $r_{\text{Silane-Ga2O3}}$. The bonding strength for various Ga—X (X represents Cl, S, N, O) bonds is listed in **Table 1**. Higher bonding energy indicates stronger interaction between two atoms. Hence, the bonding strength of Ga—X bonds could be used to represent the interaction strength between various terminal groups of silane molecules and Ga_2O_3. The Ga—O bond represents the unmodified condition, since the unmodified CuPs are partially oxidized when they get exposed to air, and the oxygen atoms at the CuP surface can interact with Ga_2O_3 through the Ga—O bond during the mixing process. Close examination of the bonding energies listed in the Table 1 reveals that the bonding energy variation of Ga—X from the highest Ga—Cl bond to the lowest Ga—N bond fits well with the trend of measured composite thermal conductivity from the highest (EGaIn-CuP@Cl composites) to the lowest (EGaIn-CuP@NH_2 composites). The similar binding energies of Ga—O and Ga—S bonds correspond to the similar thermal conductivity of EGaIn-CuP@SH and EGaIn-CuP composites. These data show that the thermal conductivity of liquid metal composites can be successfully tailored by varying the strength of chemical interactions at CuP/Ga_2O_3 interfaces, demonstrating the flexibility of this approach. We conducted the thermal conductivity measurement of EGaIn-CuP@NH_2 composites with different filler volume fractions (Figure S10, Supporting Information). The decrement factor of EGaIn-CuP@NH_2 relative to EGaIn-CuP shows an increasing trend with increasing volume fraction. This trend is possibly owing to the increasing number of CuP/Ga_2O_3 interfaces, the effect of increased r_{int} at CuP/Ga_2O_3 interfaces becomes more pronounced due to a large number of CuP/Ga_2O_3 interfaces present at high volume fractions.

COMSOL multiphysics was also utilized to theoretically investigate the influence of interfacial thermal conductance on the bulk thermal conductivity of EGaIn composites with 51 vol% modified and unmodified CuP. For the sake of simplicity, the 2D models were used to simulate the thermal conductivity of the composite. The steady-state simulation was performed in a 1000 um × 1000 um square region. Details of

Table 1. Standard bond energies of diatomic molecules Ga—X (X refer to Cl, S, O, N atoms, respectively) at 298 K.

Chemical bonding	Standard bond energy at 298 K, D°_{298}[kJ mol^{-1}]
Ga—Cl	481 ± 13[55]
Ga—S	363.9[56]
Ga—O	353.5 ± 41.8[55]
Ga—N	218.4[57,58]

the models and the parameters of the simulation are described in the supporting information. We use the gap thermal conductance parameter in COMSOL to represent the interfacial thermal conductance at CuP/Ga_2O_3 interface. By changing the value of gap thermal conductance, the bulk thermal conductivity (κ_{bulk}) of EGaIn-based composites as a function of interfacial thermal conductance (κ_{int}) can be acquired in Figure S11, Supporting Information. According to the experimentally measured κ_{bulk} of EGaIn-Cu-51 vol% composite (57.0 W m^{-1} K^{-1}) and EGaIn-CuP@Cl-51 vol% composite (64.8 W m^{-1} K^{-1}), the corresponding κ_{int} can be obtained as 6×10^6 W m^{-2} K^{-1} and 1.2×10^7 W m^{-2} K^{-1} respectively, which means the introduction of CPTES as the surface modification agent increases the κ_{int} by twofold. We can also observe that κ_{bulk} increases rapidly at the initial stage as the κ_{int} increases, however, the increasing rate keeps decreasing. When κ_{int} is large enough, the κ_{bulk} becomes relatively stable and is almost unaffected by the change of κ_{int}. The transitional state analysis was also performed to gain insight into different heat conduction processes in the EGaIn-CuP@Cl composite compared with pure EGaIn. As for EGaIn-CuP@Cl composite, Figure 3e shows that the isothermal line always propagates along with the outer rim of CuPs due to the faster heat conduction in CuP than EGaIn matrix. The transfer of heat flux symbolized by white arrows shows that the heat tends to transfer within CuPs with higher thermal conductivity. In comparison, the heat transfers uniformly in pure EGaIn as a straight isothermal line. A much slower heat flux transfer in EGaIn-CuP composite is also observed from the temperature distribution map, because of the relatively low thermal conductivity of pure EGaIn.

The formation of $CuGa_2$ IMCs consumes Ga from the EGaIn matrix, resulting in gradual solidification, surface roughening, and thermal performance deterioration of liquid metal composites.[11] Hence, inhibiting the formation rate of $CuGa_2$ IMC is the main approach to extend the stability of EGaIn-CuP pastes. In this work, the stability of EGaIn-CuP@Cl composites has been well improved, since the silane molecular layer anchored on metallic fillers could suppress the growth of $CuGa_2$ in the liquid metal matrix. The optical appearance of EGaIn-CuP and EGaIn-CuP@Cl were taken over a period of time from 1 to 10 days after mixing at room temperature (**Figure 4a**). One day after initially mixing, there was no significant difference between EGaIn-CuP and EGaIn-CuP@Cl. They all appeared as homogeneous pastes with a reflective metallic luster. After 10 days, the metallic luster completely disappeared for EGaIn-CuP composite and obvious surface roughening could be observed. In contrast, the EGaIn-CuP@Cl composite still maintained some of the metallic luster. A distinguished difference could be observed with the re-shearing of these two composites after they were stored for 10 days. EGaIn-CuP composite split into solid pieces because of the massive formation of brittle, solid $CuGa_2$ IMCs and the consumption of EGaIn. In comparison, EGaIn-CuP@Cl composite still maintained its paste-like state, implying much less consumption of EGaIn than that in EGaIn-CuP composites. Further stability evaluation experiments of our sample for the continuous 20-day incubation indicate that the EGaIn-CuP@Cl composite still maintains a homogenous paste structure and shows the suppression of $CuGa_2$ alloy formation (Figure S12, Supporting Information).

Figure 4b–d reveals the evolution of morphologies and microstructures with time in these two types of composites. There was no apparent difference between the two composites stored for 1 day after mixing, which is consistent with the optical appearance in Figure 4a. Elemental distribution by EDS mapping shows the presence of copper, gallium elements as well as the absence of indium elements in the tetragonal area, confirming the chemical composition of $CuGa_2$ (Figure 4c). After 10 days, the matrix of EGaIn-CuP composite was almost filled by $CuGa_2$ IMCs. In contrast, there were few $CuGa_2$ blocks in the EGaIn-CuP@Cl composite (Figure 4d). We also performed EDS mapping of the EGaIn-CuP and EGaIn-CuP@Cl samples stored from 1 to 10 days to show the distribution of Cu, O, Cl elements presented in the composite (Figure S13, Supporting Information). To further investigate the formation of $CuGa_2$ and stability of composites more quantitatively, X-ray diffraction (XRD) was employed to determine the intensity of characteristic $CuGa_2$ peaks in liquid metal composites. As shown in Figure 4e, the $CuGa_2$ peaks in EGaIn-CuP composite exhibit a large increase from 1 to 10 days after mixing. The faster formation of $CuGa_2$ IMCs consumes liquid gallium and increases the surface roughness of the paste, accounting for the rapidly fading metallic luster observed on the surface of EGaIn-CuP paste (Figure 4a). As for EGaIn-CuP@Cl composites, the increase of $CuGa_2$ peak intensity is much slower than that in EGaIn-CuP, indicating that enhanced stability could be achieved by chemically modifying CuP filler with silane molecules.

The mechanism lying behind the enhanced stability by silane modification can be attributed to the bonding-induced atomic diffusion impedance, which is also a bonding-mediated effect similar to the aforementioned mechanism of thermal conductivity enhancement. The silane can be strongly bonded to the CuP surface via covalent Si—O—Cu bonds. Such strong interaction not only contributes to a better thermal transport at the Cu/organic silane interface, but also helps prevent metal-metal contact.[39,59] There have been reports that investigated the diffusion barriers for electronics utilizing organic silane nanolayers. The silanes are terminated with strong electron-withdrawing groups to immobilize copper atoms through electrostatic interactions. The diffusion of copper atoms into silica is therefore restricted and the operational stability of the devices is increased as a consequence.[60–62] The same principle can also be applied to this system. The chlorine termini on the surface of CuPs have a strong electrostatic interaction with gallium atoms due to their strong electron-withdrawn effect, which helps prevent the diffusion of gallium atoms into the copper phase. With the reduced diffusion of both copper and gallium atoms, the formation of $CuGa_2$ IMCs is effectively suppressed, and the as-synthesized EGaIn-CuP@Cl composite exhibits enhanced stability.

The stability of EGaIn-CuP composites modified with NH_2 and SH terminated silane was also investigated. The XRD spectra of EGaIn-CuP@NH_2 and EGaIn-CuP@SH composites show that the increment of $CuGa_2$ peak intensity is smaller compared to the situation in unmodified composites (Figure S14, Supporting Information). The optical images (Figure S14, Supporting Information) also revealed the suppression effect of $CuGa_2$ formation by the other silanes with NH_2 and SH as

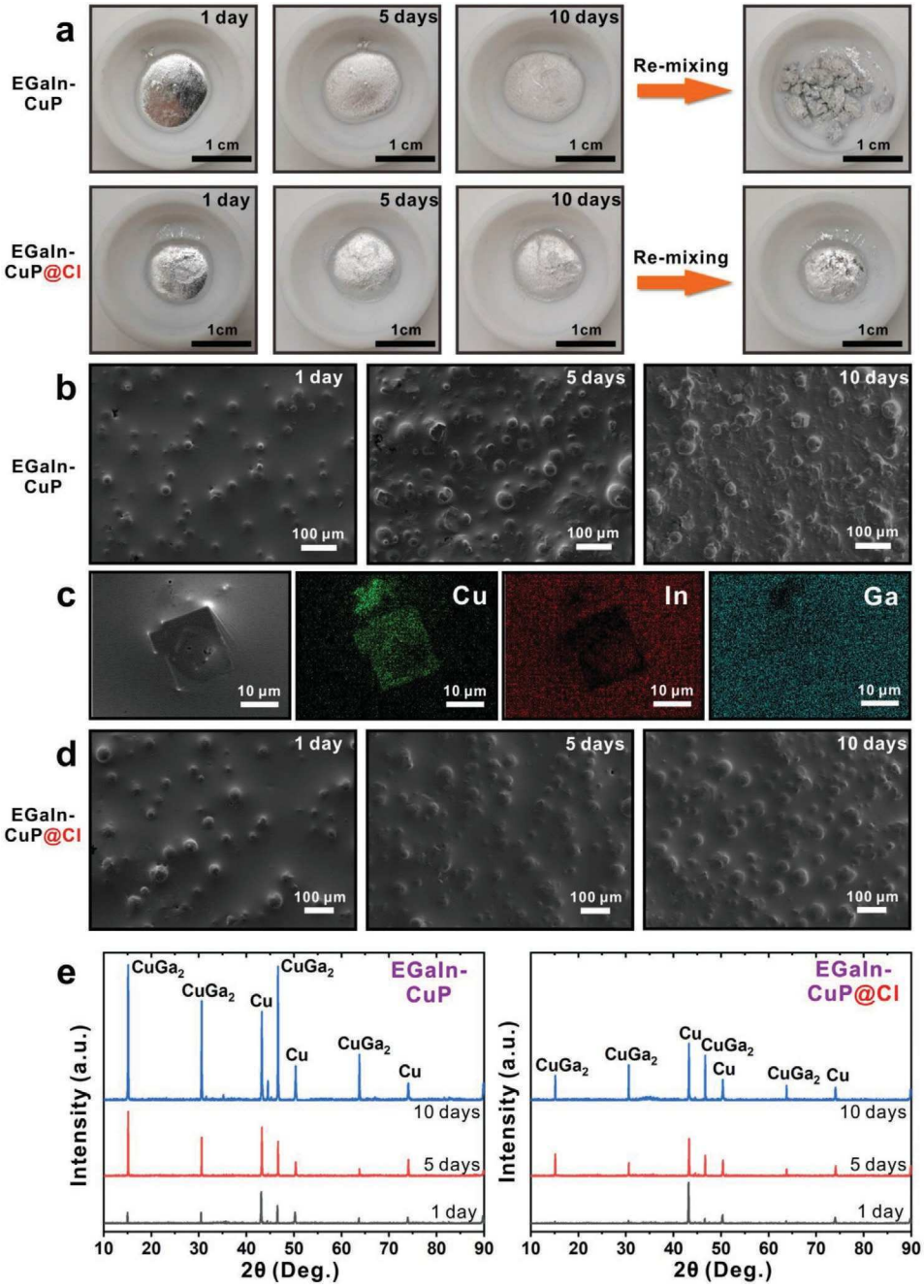

Figure 4. Stability evaluation of EGaIn-CuP@Cl and EGaIn-CuP composites. a) Optical images of EGaIn-CuP@Cl and EGaIn-CuP appearance change with storage time from 1 to 10 days. The morphologies after re-shearing the 10 day's sample are shown to further illustrate the stability difference between two composites. b) SEM images of EGaIn-CuP composite from 1 to 10 days after initial mixing. c) SEM image and EDS mapping of $CuGa_2$ alloy structure presented in EGaIn-CuP composite 5 days after mixing. d) SEM images of EGaIn-CuP@Cl composite from 1 to 10 days after initial mixing. e) XRD spectra of EGaIn-CuP and EGaIn-CuP@Cl composites from 1 to 10 days after initial mixing.

terminal groups. After re-shearing the composites stored for 10 days, EGaIn-CuP@NH_2 and EGaIn-CuP@SH composites still maintained their paste-like state because of suppressed formation of $CuGa_2$ IMCs in the LM matrix. The stability enhancement in EGaIn-CuP@NH_2 and EGaIn-CuP@SH can be simply explained by the formation of diffusion barriers at the interface of CuP and EGaIn matrix. The surface modification using both silanes would introduce a thin organic layer at the interface of CuP and EGaIn matrix. Such an organic layer would serve as a physical diffusion barrier impeding the diffusion of Cu and Ga atoms, and thus slowed down the formation of $CuGa_2$ IMCs.

For practical TIM applications, the stability of liquid metal TIM at elevated temperatures should be also investigated. Therefore, we carried out the stability evaluation of EGaIn-CuP@Cl composite stored for 10 days at 60 °C, which falls in the working temperature range of most electronic devices

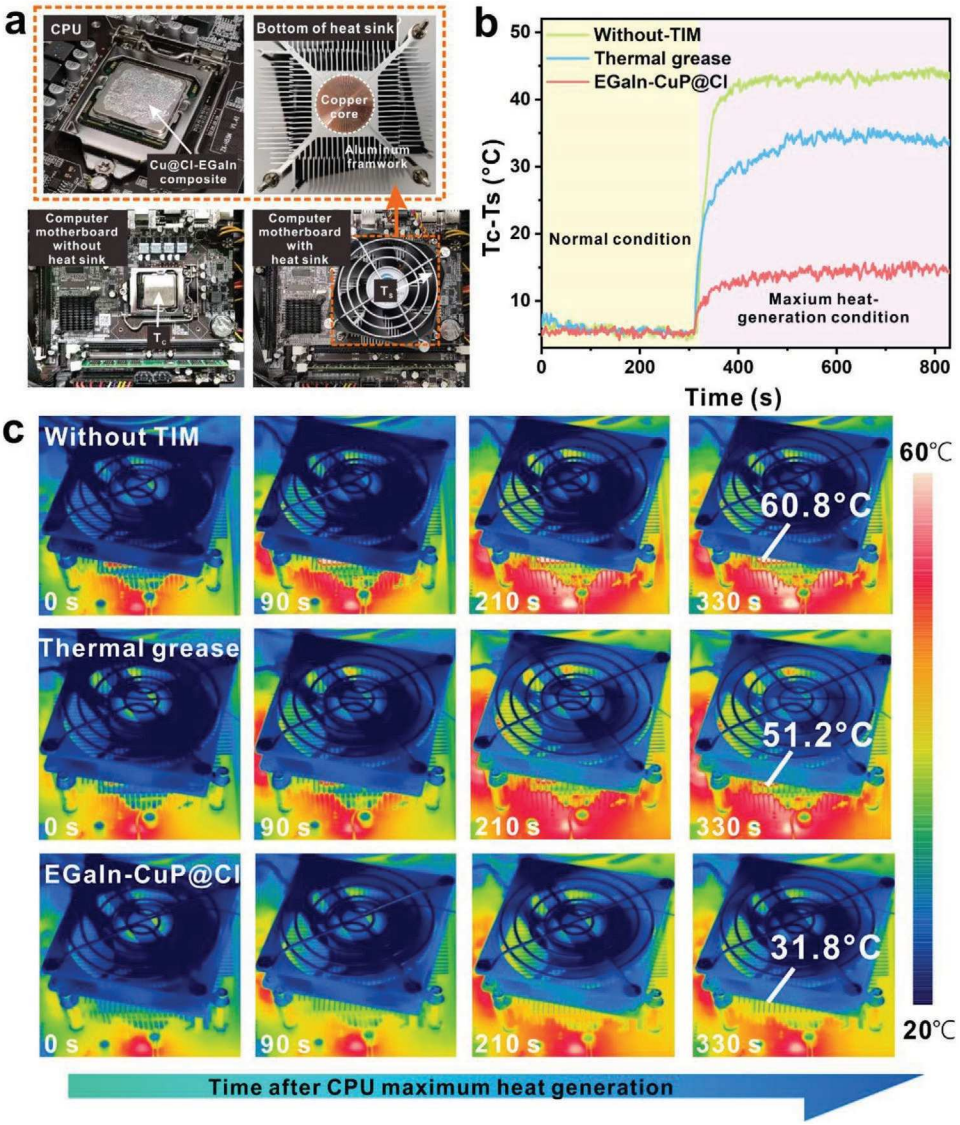

Figure 5. Computer CPU heat dissipation test using EGaIn-CuP@Cl composite as TIM. a) Optical images of computer motherboard before and after heat sink installation. Images in the enlarged dotted frame show both the optical image of CPU after applying EGaIn-CuP@Cl composites and the bottom of the heat sink with a copper core. b) Temperature profiles of T_c-T_s before and after maximum CPU heat generation (T_c: CPU surface temperature, T_s: ambient environment temperature). Three situations (without TIMs, thermal grease application, EGaIn-CuP@Cl composite application) were investigated. c) Comparison of temporal infrared images of the motherboard after maximum heat generation with no-TIM, thermal grease, and EGaIn-CuP@Cl composite.

and TIMs. XRD spectra show that the $CuGa_2$ peak intensity in EGaIn-CuP@Cl composite stored at 60 °C increased faster compared with the same composite stored at room temperature (Figure S15, Supporting Information). It is attributed to the more rapid diffusion of metallic atoms at higher temperature, signifying a faster formation of $CuGa_2$ IMCs. Though the $CuGa_2$ IMC formation rate has been promoted at high temperature, it still maintained a paste-like rheology instead of splitting into solid pieces observed in EGaIn-CuP composite (Figure 4a). The high-temperature control experiments further confirm that the EGaIn-CuP@Cl composite exhibits a greatly enhanced stability compared with unmodified EGaIn-CuP composite, demonstrating its potential in practical TIM applications.

To demonstrate the feasibility of using EGaIn-CuP@Cl composite in thermal management applications, a heat dissipation experiment with a desktop computer CPU was performed, and EGaIn-CuP@Cl-51 vol% composite was utilized as TIMs (**Figure 5a**). Compared with pure liquid metal, the EGaIn-CuP@Cl-51 vol% composite could be easily applied to the CPU chip (Figure S16, Supporting Information). The heat sink with a fan was attached to the top of CPU. The temperatures on the top surface (T_c) of CPU and ambient air above the heat sink (T_s) were measured by two T-type thermocouples. The CPU maximum heat generation using Prime 95 software was started at around 300 s. The change of temperature difference between T_c and T_s (T_c-T_s) before and after the maximum heat generation

is shown in Figure 5b. The initial temperature differences with and without TIM are almost the same before the start of the test. After arriving at the maximum heat generation, the temperature difference (T_c-T_s) is the greatest without applying TIM between CPU and heat sink, rapidly rising from an initial 5.1 °C to an equilibrium temperature of 43.6 °C. The application of commercial thermal grease (Shin-Etsu X-23-7783-D, 6 W m^{-1} K^{-1}) lowers the temperature difference to 34.0 °C after the maximum heat generation. In comparison, the EGaIn-CuP@Cl-51 vol% composite lowers T_c-T_s to 14.7 °C, achieving a significant heat dissipation improvement over the commercial thermal grease. To better visualize the thermal dissipation performance, the infrared (IR) camera was used to record the temperature change around the CPU and heat sink from 0 s to 330 s after the start of the maximum heat generation. Figure 5c clearly shows that after the application of the EGaIn-CuP@Cl-51 vol% composite, the area of high-temperature region in the thermal image is significantly suppressed compared to the cases with no-TIM and commercial thermal grease.

To gain insight into the interface contact condition between our LM composite and solid substrate in the TIM applications, we employed Micro-CT analysis. After applying the EGaIn-CuP@Cl composite between two copper foils, such sandwich-like structure was compressed with an external force exerted to simulate the actual loading condition of heat sinks to the TIM materials. This structure was then characterized by micro-CT to simulate the interface contact in the TIM applications. The cross-section of the sandwich-like structure was shown in Figure S17, Supporting Information, few air gaps (less than 4%) can be seen at the interfaces between copper foils and liquid metal composite, and the composite shows close contact with the copper foils, indicating a small interface contact resistance and its potential to be used as an effective TIM.

3. Conclusion

In this work, we have successfully synthesized the liquid metal-copper composite with enhanced thermal conductivity and stability via silane surface modification of CuP fillers. Such silanes with chlorine groups at the terminus serve as molecular thermal linkers at CuP/Ga_2O_3 interfaces. A thermal conductivity as high as 65.9 W m^{-1} K^{-1} has been achieved using this interfacial engineering approach. It is among the highest value ever reported for liquid metal-metallic filler composites. The silane molecules capped on the CuP also form diffusion barriers between copper and EGaIn matrix, which largely slows down the alloy formation rate and enhances the stability of composites. The CPU heat dissipation test demonstrated the thermal performance of EGaIn-CuP@Cl composite, with a steady-state temperature difference of 14.1 °C between T_c and T_s, a close to 20 °C reduction over the commercial thermal grease. The interfacial engineering process established in this work also offers an alternative approach for the fabrication of high-performance liquid metal composites, which may further advance their applications in various areas including thermal management systems, flexible electronics, consumer electronics, and biomedical systems.

Supporting Information

Supporting Information is available from the Wiley Online Library or from the author.

Acknowledgements

The authors are grateful for financial support by National Key R & D Project from Minister of Science and Technology of China (Grant No. 2017YFB0406000), the National Natural Science Foundation of China (Grant Nos. 51973109, 51521004, and 51873105), the 111 Project (Grant No. B16032), the Innovation Program of Shanghai Municipal Education Commission (Grant No. 2019-01-07-00-02-E00069), and the Center of Hydrogen Science of Shanghai Jiao Tong University. M.D.D. is grateful for the support from the National Science Foundation (ASSIST, EEC-1160483, and CMMI- 2032409). The authors acknowledge the Instrumental Analysis Center and the Zhiyuan Innovative Research Center of Shanghai Jiao Tong University for providing SEM, XRD, DSC, and LFA analysis.

Conflict of Interest

The authors declare no conflict of interest.

Data Availability Statement

All the data are shared within the manuscript and the Supporting Information.

Keywords

chemical modification, intermetallic compounds, liquid metals, thermal conductivity

Received: April 23, 2021
Revised: August 10, 2021
Published online:

[1] Y. Zhang, N. Hao, X. Lin, S. Nie, *Carbohydr. Polym.* **2020**, *234*, 115888.
[2] J. Hansson, T. M. J. Nilsson, L. Ye, J. Liu, *Int. Mater. Rev.* **2017**, *63*, 22.
[3] K. M. Razeeb, E. Dalton, G. L. W. Cross, A. J. Robinson, *Int. Mater. Rev.* **2017**, *63*, 1.
[4] Y. Zhang, J. Ma, N. Wei, J. Yang, Q. X. Pei, *Phys. Chem. Chem. Phys.* **2021**, *23*, 753.
[5] M. Zadan, C. Chiew, C. Majidi, M. H. Malakooti, *Multifunct. Mater.* **2021**, *4*, 012001.
[6] K. Huang, W. Qiu, M. Ou, X. Liu, Z. Liao, S. Chu, *RSC Adv.* **2020**, *10*, 18824.
[7] K.-Q. Ma, J. Liu, *Phys. Lett. A* **2007**, *361*, 252.
[8] M. D. Dickey, R. C. Chiechi, R. J. Larsen, E. A. Weiss, D. A. Weitz, G. M. Whitesides, *Adv. Funct. Mater.* **2008**, *18*, 1097.
[9] N. Kazem, T. Hellebrekers, C. Majidi, *Adv. Mater.* **2017**, 29.
[10] K. Doudrick, S. Liu, E. M. Mutunga, K. L. Klein, V. Damle, K. K. Varanasi, K. Rykaczewski, *Langmuir* **2014**, *30*, 6867.
[11] W. Kong, Z. Wang, M. Wang, K. C. Manning, A. Uppal, M. D. Green, R. Y. Wang, K. Rykaczewski, *Adv. Mater.* **2019**, *31*, 1904309.

[12] C. Wang, Y. Gong, B. V. Cunning, S. Lee, Q. Le, S. R. Joshi, O. Buyukcakir, H. Zhang, W. K. Seong, M. Huang, M. Wang, J. Lee, G. H. Kim, R. S. Ruoff, *Sci. Adv.* **2021**, *7*, eabe3767.
[13] J. Tang, X. Zhao, J. Li, R. Guo, Y. Zhou, J. Liu, *ACS Appl. Mater. Interfaces* **2017**, *9*, 35977.
[14] S. Ki, J. Shim, S. Oh, E. Koh, D. Seo, S. Ryu, J. Kim, Y. Nam, *Int. J. Heat Mass Transfer* **2021**, *170*, 121012.
[15] Z. Lin, H. Liu, Q. Li, H. Liu, S. Chu, Y. Yang, G. Chu, *Appl. Phys. A* **2018**, *124*, 368.
[16] Y. Lu, Z. Che, F. Sun, S. Chen, H. Zhou, P. Zhang, Y. Yu, L. Sheng, J. Liu, *ACS Appl. Mater. Interfaces* **2021**, *13*, 5256.
[17] S. Wei, Z. F. Yu, L. J. Zhou, J. D. Guo, *J. Mater. Sci.: Mater. Electron.* **2019**, *30*, 7194.
[18] S. Chen, H.-Z. Wang, R.-Q. Zhao, W. Rao, J. Liu, *Matter* **2020**, *2*, 1446.
[19] S. Chen, Z. Deng, J. Liu, *Nanotechnology* **2021**, *32*, 092001.
[20] D. P. Parekh, C. M. Fancher, M. G. Mohammed, T. V. Neumann, D. Saini, J. Guerrier, C. Ladd, E. Hubbard, J. L. Jones, M. D. Dickey, *ACS Appl. Nano Mater.* **2020**, *3*, 12064.
[21] D. K. Sarfo, R. R. Taylor, A. P. O'Mullane, *ACS Appl. Electron. Mater.* **2020**, *2*, 2921.
[22] A. L. Lereu, F. Lemarchand, M. Zerrad, M. Yazdanpanah, A. Passian, *J. Appl. Phys.* **2015**, *117*, 063110.
[23] M. V. Trenikhin, A. V. Bubnov, A. G. Kozlov, A. I. Nizovskii, V. K. Duplyakin, *Russ. J. Phys. Chem.* **2006**, *80*, 1110.
[24] O. I. Tikhomirova, M. V. Pikunov, I. D. Marchukova, I. N. Tochenova, I. P. Izotova, *Sov. Mater. Sci.* **1972**, *5*, 355.
[25] S.-J. Hong, C. Suryanarayana, *J. Appl. Phys.* **2004**, *96*, 6120.
[26] I. A. De Castro, A. F. Chrimes, A. Zavabeti, K. J. Berean, B. J. Carey, J. Zhuang, Y. Du, S. X. Dou, K. Suzuki, R. A. Shanks, R. Nixon-Luke, G. Bryant, K. Khoshmanesh, K. Kalantar-Zadeh, T. Daeneke, *Nano Lett.* **2017**, *17*, 7831.
[27] R. Guo, X. Wang, H. Chang, W. Yu, S. Liang, W. Rao, J. Liu, *Adv. Eng. Mater.* **2018**, *20*, 1800054.
[28] R. Guo, B. Cui, X. Zhao, M. Duan, X. Sun, R. Zhao, L. Sheng, J. Liu, J. Lu, *Mater. Horiz.* **2020**, *7*, 1845.
[29] X. Wang, W. Yao, R. Guo, X. Yang, J. Tang, J. Zhang, W. Gao, V. Timchenko, J. Liu, *Adv. Healthcare Mater.* **2018**, *7*, 1800318.
[30] K. C. Vrancken, L. De Coster, P. Van Der Voort, P. J. Grobet, E. F. Vansant, *J. Colloid Interface Sci.* **1995**, *170*, 71.
[31] P. Silberzan, L. Leger, D. Ausserre, J. J. Benattar, *Langmuir* **2002**, *7*, 1647.
[32] E. McCafferty, J. P. Wightman, *Surf. Interface Anal.* **1998**, *26*, 549.
[33] M. Forster, R. Raval, J. Carrasco, A. Michaelides, A. Hodgson, *Chem. Sci.* **2012**, *3*, 93.
[34] F. Adam, M. S. Batagarawa, *Appl. Catal., A* **2013**, *454*, 164.
[35] H. Jiang, Z. Zheng, Z. Li, X. Wang, *Ind. Eng. Chem. Res.* **2006**, *45*, 8617.
[36] G. Beamson, D. Briggs, *High Resolution XPS of Organic Polymers: The Scienta ESCA300 Database*, Wiley, New York **1992**.
[37] R. Krumpolec, T. Homola, D. Cameron, J. Humlíček, O. Caha, K. Kuldová, R. Zazpe, J. Přikryl, J. Macak, *Coatings* **2018**, *8*, 369.
[38] M. P. Seah, *Surf. Interface Anal.* **2012**, *44*, 1353.
[39] G. Ramanath, G. Cui, P. G. Ganesan, X. Guo, A. V. Ellis, M. Stukowski, K. Vijayamohanan, P. Doppelt, M. Lane, *Appl. Phys. Lett.* **2003**, *83*, 383.
[40] W. Kong, N. U. H. Shah, T. V. Neumann, M. H. Vong, P. Kotagama, M. D. Dickey, R. Y. Wang, K. Rykaczewski, *Soft Matter* **2020**, *16*, 5801.
[41] M. D. Bartlett, N. Kazem, M. J. Powell-Palm, X. Huang, W. Sun, J. A. Malen, C. Majidi, *Proc. Natl. Acad. Sci. U. S. A.* **2017**, *114*, 2143.
[42] M. D. Losego, M. E. Grady, N. R. Sottos, D. G. Cahill, P. V. Braun, *Nat. Mater.* **2012**, *11*, 502.
[43] P. J. O'Brien, S. Shenogin, J. Liu, P. K. Chow, D. Laurencin, P. H. Mutin, M. Yamaguchi, P. Keblinski, G. Ramanath, *Nat. Mater.* **2013**, *12*, 118.
[44] F. Sun, T. Zhang, M. M. Jobbins, Z. Guo, X. Zhang, Z. Zheng, D. Tang, S. Ptasinska, T. Luo, *Adv. Mater.* **2014**, *26*, 6093.
[45] X. Wei, T. Zhang, T. Luo, *ACS Energy Lett.* **2017**, *2*, 2283.
[46] M. J. Regan, H. Tostmann, P. S. Pershan, O. M. Magnussen, E. DiMasi, B. M. Ocko, M. Deutsch, *Phys. Rev. B* **1997**, *55*, 10786.
[47] S. Li, C. Yang, J. Zhang, L. Dong, C. Cai, H. Liang, W. Liu, *Nanomaterials* **2020**, *10*, 1760.
[48] J. Lu, K. Yuan, F. Sun, K. Zheng, Z. Zhang, J. Zhu, X. Wang, X. Zhang, Y. Zhuang, Y. Ma, X. Cao, J. Zhang, D. Tang, *ACS Appl. Mater. Interfaces* **2019**, *11*, 42708.
[49] Z. Wang, J. A. Carter, A. Lagutchev, Y. K. Koh, N. H. Seong, D. G. Cahill, D. D. Dlott, *Science* **2007**, *317*, 787.
[50] S. Shen, A. Henry, J. Tong, R. Zheng, G. Chen, *Nat. Nanotechnol.* **2010**, *5*, 251.
[51] A. Henry, G. Chen, *Phys. Rev. Lett.* **2008**, *101*, 235502.
[52] J. G. McLean, P. Kruse, G.-P. Jiang, H. E. Ruda, A. C. Kummel, *J. Phys. Chem. A* **1999**, *103*, 10364.
[53] A. Shanker, C. Li, G. H. Kim, D. Gidley, K. P. Pipe, J. Kim, *Sci. Adv.* **2017**, *3*, e1700342.
[54] T. V. Kulikova, V. A. Bykov, K. Y. Shunyaev, A. B. Shubin, *Defect Diffus. Forum* **2012**, *326–328*, 227.
[55] D. R. Lide, *CRC Handbook of Chemistry and Physics*, CRC Press, Boca Raton, FL **2005**.
[56] J. J. BelBruno, E. Sanville, A. Burnin, A. K. Muhangi, A. Malyutin, *Chem. Phys. Lett.* **2009**, *478*, 132.
[57] J. Nord, K. Albe, P. Erhart, K. Nordlund, *J. Phys.: Condens. Matter* **2003**, *15*, 5649.
[58] A. R. Smith , R. M. Feenstra , *J. Vac. Sci. Technol., B: Microelectron. Nanometer Struct.–Process., Meas., Phenom.* **1998**, *16*, 2242.
[59] Y. Wang, Z. Wang, L. Zhao, Q. Fan, X. Zeng, S. Liu, W. K. Pang, Y. B. He, Z. Guo, *Adv. Mater.* **2021**, *33*, 2008133.
[60] P. G. Ganesan, A. P. Singh, G. Ramanath, *Appl. Phys. Lett.* **2004**, *85*, 579.
[61] D. D. Gandhi, U. Tisch, B. Singh, M. Eizenberg, G. Ramanath, *Appl. Phys. Lett.* **2007**, *91*, 143503.
[62] D. D. Gandhi, P. G. Ganesan, V. Chandrasekar, Z. Gan, S. G. Mhaisalkar, H. Li, G. Ramanath, *Appl. Phys. Lett.* **2007**, *90*, 163507.